Cerebral Cortex, April 2018;28: 1168–1182

doi: 10.1093/cercor/bhx028
Advance Access Publication Date: 10 March 2017
Original Article

ORIGINAL ARTICLE

Reciprocal Connections Between Cortex and Thalamus Contribute to Retinal Axon Targeting to Dorsal Lateral Geniculate Nucleus

Yupu Diao[1,†], Liyuan Cui[1,†], Yuqing Chen[1], Timothy J. Burbridge[2], Wenqi Han[2], Brunhilde Wirth[3], Nenad Sestan[2], Michael C. Crair[2] and Jiayi Zhang[1]

[1]Institutes of Brain Science, State Key Laboratory of Medical Neurobiology, and Collaborative Innovation Center for Brain Science, Fudan University, Shanghai 200 032, China, [2]Department of Neuroscience, Yale School of Medicine, New Haven, CT 06 510, USA and [3]Institute of Human Genetics, Institute for Genetics, Center for Molecular Medicine Cologne, University of Cologne, Cologne 55322, Germany

Address correspondence to Jiayi Zhang, School of Medicine, Fudan University, Rm. 1006, Mingdao Building, 131 Dongan Rd, Shanghai 200 032, China. Email: jiayizhang@fudan.edu.cn

[†]Yupu Diao and Liyuan Cui contributed equally to this work

Abstract

The dorsal Lateral Geniculate Nucleus (dLGN) is the primary image-forming target of the retina and shares a reciprocal connection with primary visual cortex (V1). Previous studies showed that corticothalamic input is essential for the development of thalamocortical projections, but less is known about the potential role of this reciprocal connection in the development of retinal projections. Here, we show a deficit of retinal innervation in the dLGN around E18.5 in Tra2β conditional knockout (cKO) "cortexless" mice, an age when apoptosis occurs along the thalamocortical tract and in some dLGN neurons. *In vivo* electrophysiology experiments in the dLGN further confirmed the loss of functional retinal input. Experiments with *N*-methyl-d-aspartic acid-induced V1 lesion as well as *Fezf2* cKO mice confirmed that the disruption of connections between the dLGN and V1 lead to abnormal retinal projections to the dLGN. Interestingly, retinal projections to the ventral Lateral Geniculate Nucleus (vLGN) and Superior Colliculus (SC) were normal in all 3 mice models. Finally, we show that the cortexless mice had worse performance than control mice in a go-no go task with visual cues. Our results provide evidence that the wiring of visual circuit from the retina to the dLGN and V1 thereafter is coordinated at a surprisingly early stage of circuit development.

Key words: corticogeniculate connections, dLGN, retinofugal projection, SC

Introduction

The development of a functional neural circuit requires precise targeting and elaboration of long-range projecting axons. The visual system has been a long-standing model for studying the precise wiring of neural circuits. Much progress has been made toward learning how retinal axons initially path find and eventually form precise retinotopic and eye-specific maps in their targets (Huberman et al. 2008). Axon guidance cues that are expressed in both the retina and image-forming targets such as the dorsal Lateral Geniculate Nucleus (dLGN; Feldheim and O'Leary, 2010) cooperate with spatiotemporally patterned spontaneous neural activity (Ackman et al. 2012) to give rise to precisely wired circuits. One remaining question concerns the mechanism whereby retinal axons identify and initially project to their target nuclei, as well as how they preferentially elaborate and refine within specific regions of those

nuclei (Cruz-Martín et al. 2014). Recent studies have indicated that specific retinal ganglion cells (RGCs) and neurons in their non-image-forming target nuclei can express the same guidance molecules, the deletion of which causes defects in retinal axon targeting (Osterhout et al. 2011; Osterhout et al. 2015), but it is unknown whether coincident projections to these targets in image-forming nuclei also contributes to this process.

dLGN relays visual information from the RGCs to the visual cortex and receives feedback projections from the cortex, comprising a reciprocal circuit (Briggs and Usrey 2007, 2011; Seabrook et al. 2013). Early studies showed that visual cortex lesion in newborn and juvenile cats and monkeys leads to reorganization of retinogeniculate synapses and loss of RGCs (Weller and Kaas 1980; Wilkes et al. 1985; Kalil and Behan 1987; Boire et al. 2000). Similar cortical lesions in adult prosimian primate did not cause defects in retinogeniculate projections or in the retina (Weller et al. 1981), suggesting that cortex plays a role in the early postnatal organization of retinogeniculate synapses. In mice, cortical axons interact with and guide thalamic axons in subpallium/pallium at around E14.5 (Deck et al. 2013) and approach dLGN at E18.5 (Hevner et al. 2002). Axons from the majority of cortical neurons begin to innervate LGN at P3 (Brooks et al. 2013; Seabrook et al. 2013; Grant et al. 2016), while retinal axons enter dLGN before E15.5 and arborize and refine through eye-opening at P12–13. Guido, Fox and colleagues showed that retinal input prevented cortical axons from entering the dLGN by regulating aggrecanase expression in the dLGN before P2, suggesting that retinal and cortical innervation of the dLGN is coordinated (Brooks et al. 2013; Seabrook et al. 2013). Shanks et al. demonstrated that cortex is essential for RGC axons to terminate in the dLGN and mice without V1 can still perform a number of visual tasks (Shanks et al. 2016). How cortex is involved in retinal axon targeting in the dLGN and the contribution of dLGN-V1 versus SC in visual functions remains unknown.

Alternative splicing factor transformer 2 beta (*Tra2β*) is known to participate in many biological processes including neuronal development (Watermann et al. 2006; Li et al. 2007). Deletion of *Tra2β* is lethal at ~E8 in mice (Mende et al. 2010). Here we used *Tra2β*$^{fl/fl}$; *Emx1-Cre* mice (Mende et al. 2010) as a "cortexless" mouse model, in which a majority of cortical areas are absent during embryogenesis (Roberts et al. 2014). We find that the innervation of retinal axons in dLGN was greatly reduced as early as E18.5, leaving all other retinofugal projections largely unaffected including vLGN and SC. Cleaved caspase-3 was specifically expressed in thalamocortical tract and some dLGN neurons but not in the vLGN or SC at E16.5 and E18.5. Pharmacological lesion in V1 at E16.5 demonstrated that the projections from the retina to dLGN but not SC were disrupted when cortex was removed. Further, major loss of corticogeniculate connections in *Fezf2* conditional knockout (cKO) mice with otherwise normal cortex also resulted in a disruption in retinogeniculate but not retinocolliculi projections. Interestingly, without the retina-dLGN-V1 circuit, *Tra2β* cKO mice did not distinguish gratings with 2 perpendicular orientations in a go-no go task as well as the control mice. These results suggest that the development of retinogeniculate projections relies in part on early reciprocal connections between visual cortex and the dLGN.

Materials and Methods

Animals and Genotyping

Tra2β$^{fl/fl}$ mice were provided by Prof. Brunhilde Wirth as a gift (Institute of Human Genetics, University of Cologne). *Emx1-Cre* mice were purchased from the Jackson laboratory (https://www.jax.org/strain/005628). *TdTomato*$^{fl/fl}$ mice were also purchased from the Jackson laboratory (https://www.jax.org/strain/007914). *Fezf2*$^{fl/fl}$ mice were generated as previously described (Han et al. 2011). CAG-*Cat-Gfp* mice were provided as a gift (Kawamoto et al. 2000). All animals were raised and bred at 25 °C, 50% relative humidity, 12 h light and dark cycles. *Tra2β*$^{fl/fl}$ homozygous mice were bred with *Emx1-Cre* homozygous mice to produce the first heterozygous generation whose genotype was *Tra2β*$^{fl/+}$; *Emx1-Cre*. The first heterozygous generation mice were crossed to generate the second generation mice. Among the second generation pups, we used *Tra2β* homozygous and *Cre* positive mice. For genotyping the first and second generation mice, 4 pairs of primers were used. To differentiate *Tra2β*$^{fl/fl}$ knock-in from wild-type, we used primer 5′-AAGGCGTTCTAGATCAAAGTCCAG-3′ and 5′-CGAGAGGGCACGAGAGGACAATC-3′. *Tra2β*$^{fl/fl}$ had a band at 821 bp and wild-type at 950 bp. To distinguish heterozygous and homozygous *Emx1-Cre* mice, we used 2 pairs of primers, 5′-GCGGTCTGGCAGTAAAAACTATC-3′ and 5′-GTGAAACAGCATT GCTGTCACTT-3′ for *Cre* recombinase genotype, 5′-AAGGTGT GGTTCCAGAATCG-3′ and 5′-CTCTCCACCAGAAGGCTGAG-3′ for wild-type genotype, with mutant band at 102 bp, heterozygous band at 102 bp and 378 bp, and wild-type band at 378 bp. At the same time, we used another pair of primers 5′-GTAGTGAAGGT CTGTTACCC-3′ and 5′-CACCAGAAAATTTAACAAATTAAAC-3′ to check the efficiency of *Tra2β* gene knockout in *Tra2β*$^{fl/fl}$; *Emx1-Cre* mice. The knocked out band was at 256 bp.

Postnatal Intravitreous Injection and Analysis of Retinal Projections

Mice were anesthetized and 1.0–1.5 μL cholera toxin subunit β (CTB), CTB-488, CTB-555, or CTB-647 (Molecular Probes, Invitrogen, C22842, C22843, C34778) were injected into left and/or right eyes, respectively, using NanoJectII (Drummond Scientific Company). After 36–48 h, mice were perfused and the brains were fixed in 4% paraformaldehyde (PFA) overnight, followed by vibratome sectioning at 100 μm coronally for LGN slices and sagittally for SC slices. We collected 4 slices from each mouse with the largest dLGN and vLGN for further analysis. As for SC, we chose 4 consecutive slices with the first slice starting at 150 μm lateral to the midline. Images were taken under microscope (Olympus, BX51) at an auto-exposure mode with 3% spot at the brightest fluorescence area. In order to get the whole SC, 2 images with both green and red channels were taken. These images were merged and cropped to obtain images with the same pixel numbers in ImageJ.

Quantification of the retinal projections was conducted according to procedures described in previous reports (Xu et al. 2011; Zhang et al. 2012). Briefly, all images were background subtracted in ImageJ, then the fractions of contralateral, ipsilateral, and overlap projections in dLGN were calculated in Matlab using custom programs. The territory of dLGN, vLGN, and SC was outlined according to the contralateral projection. Threshold 40% (pixels with fluorescence intensity above 40% of the maximum intensity) was verified to best describe the eye-specific segregation phenotype and was chosen to measure the fractions of contralateral and ipsilateral projections. In order to systematically study the changes in LGN and SC, we also measured the physical sizes of dLGN, vLGN, and SC by counting the total number of pixels within the outlines.

Embryonic Intravitreous Injection and Analysis of Retinal Projections

Female and male *Tra2β*$^{fl/+}$; *Emx1-Cre* mice were raised separately, put in the same cage overnight, and separated again in the next morning. Vaginal plug was checked. If the female mouse was pregnant, intravitreous injection surgery was conducted at E16.5 or E18.5 in fetal mice. Briefly, the pregnant female mouse was anesthetized with isoflurane on heated pad (FHC Inc.). A 3-cm long and "1" shaped incision was carefully made around the position of womb and the embryos were pulled out carefully with forceps. Small volume of 37 °C phosphate-buffered saline (PBS) with antibiotics was applied to the embryos continuously. Each embryo was stabilized by hand softly, and the embryo was adjusted so that the eyeball was completely visible. During injection, the NanoJectII was held by hand with the glass pipette piercing through the pregnant female's uterine wall, fetal mice's skin, and sclera. Of note, 1 μL CTB-555 was injected intravitreously into one eye. The skin of the pregnant female mouse was sutured after injection. The mouse was continuously anesthetized for 10 h before the embryos were perfused with 4% PFA and the retinas were dissected to check if the dye labeled majority of the RGCs. The brains of embryos with well-labeled eyes were fixed overnight at 4 °C. In all, 20 μm slices were cut coronally for LGN and SC images. The slices were washed 5 times to remove optimal cutting temperature compound (OCT) before imaging.

Quantitative analysis of the retinal projections in E16.5 and E18.5 embryos was similar to the method used in postnatal mice. It is more difficult to define the territory of the dLGN in *Tra2β* cKO mice, due to the lack of dense retinogeniculate axons in the dLGN. Diamidino-phenyl-indole (DAPI) staining, the remaining sparse axons, vLGN, and optic tract were combined to define the territory of the dLGN. Meanwhile, DAPI staining and CTB-488 labeled axons together determined the territory of the dLGN, vLGN, and SC in control mice, as well as that of the vLGN and SC in *Tra2β* cKO mice. A lower threshold of 30% was chosen in this analysis because the slices were thinner compared with those in postnatal mice and 30% best described the phenotypes in the fluorescent images. Sizes of the dLGN, vLGN, and SC were calculated using custom software routines written in Matlab.

In Vivo Electrophysiology Recording in dLGN

The mice were anaesthetized by 1.5% isoflurane in a stereotaxic setup (RWD, China) on a heating pad. One percent lidocaine (10 mg/mL lidocaine in saline, MP Biomedicals) was injected subcutaneously under the scalp. After removal of the scalp, the position of the dLGN was marked on the skull (coordinates for control mice were mentioned in "Stereotaxic Injection in the dLGN"; for the *Tra2β* cKO mice, the dLGN was not covered by the cortex and can be recognized directly). Of note, 2 mm × 2 mm craniotomy was made. Dura was removed carefully and the craniotomy was filled with warm (37 °C) sterile buffered saline (150 mM NaCl, 2.5 mM KCl, 10 mM 4-(2-?hydroxyethyl)-1-piperazineethanesulfonic acid (HEPES), pH 7.4) throughout the experiment. Isoflurane was turned down to 0.5% to maintain a stable respiratory rate. Single electrode (World Precision Instrument) was inserted into the dLGN at a depth about 2350–2700 μm for control mice and 0–300 μm for *Tra2β* cKO mice. We advanced the electrode vertically every 30 μm and covered the whole dLGN. Whole-field stimulation was driven by Diode Pump Solid State laser (473 nm, 10–15 mW, BaiAoJin). The electrophysiology recordings were conducted as follows: a 2-min recording without any stimulus followed by 1-s stimulus and 9-s interval repeated for 20 cycles. The signals were pre-amplified (Microelectrode AC Amplifier 1800, A-M Systems, Inc.), high-pass filtered at 1 Hz and sampled at 10 kHz. After the recording, the electrode was dipped into DiI solution and inserted back to the brain at the largest recording depth to mark the recording sites in the dLGN.

We analyzed the electrophysiology data in Spike2. Signals were high-pass filtered at 300 Hz and sorted in Spike2. We set the threshold for the spike at 1.5 (signal-to-noise ratio). Sorted spikes were used to generate raster plots for the spikes activity during light stimulus. Firing rate during visual stimulus was calculated.

Immunohistochemistry

Mice were perfused with PBS and then 4% PFA (Sigma, P6148). Brains were fixed in 4% PFA overnight at 4 °C. Thirty percent sucrose was used to dehydrate the fixed brains for 2 days. The brains were embedded in OCT compound (Leica) and stored at −80 °C. In total, 30 μm slices were cut and washed with Tris-Buffered Saline for 5 times (5 min each time) to get rid of the OCT before being immersed in 0.5% Triton-X-100 for 20 min. The slices were then blocked in 10% Donkey serum for 2 h at room temperature followed by first antibody hybridization overnight at 4 °C (information for first antibodies was listed below). The slices were washed for another 5 times (5 min for each time), second antibody (Jackson ImmunoResearch) was added to the slices and incubated at room temperature for about 2 h in the dark. The slices were washed 3 times (5 min for each time), then stained in 1:3000 DAPI working solution for 7 min and washed for 2 more times. At last, slides were mounted and fluorescent images were taken.

List of first antibodies used in this study

Antibody	Host	Products (catalog no.)	Dilution
GFP	Chicken	Avēs Labs Inc. (GFP-1020)	1:1000
VGLUT1	Mouse	UC Davis/NIH NeuroMab (75–066)	1:200
TRA2β	Rabbit	Sigma (AV40528)	1:250
DsRed	Rabbit	Takara (632496)	1:800
Cleaved caspase-3	Rabbit	Cell Signaling Technology	1:400
VGLUT2	Rabbit	Synaptic Systems	1:200
FOXP2	Goat	Santa Cruz Biotechnology (21 069)	1:500
Brn3a	Goat	Santa Cruz Biotechnology	1:500
L1-CAM	Mouse	Abcam (ab24345)	1:200

Stereotaxic Injection in the dLGN

Adult mice were fixed on stereotaxic setup by nose clip and ear bars. Of note, 1 cm long and "1" shaped incision was made in the middle of the scalp. The brain was adjusted to be flat in both *x* and *y* directions. According to "The Mouse Brain" (Keith B.J. Franklin and George Paxinos, the third edition, Elsevier), bregma was defined as the origin of stereotaxic with $x = 0$, $y = 0$, $z = 0$, and lambda was defined as $x = 0$, $y = -4.2$ mm, $z = 0$. Injection coordinates for the dLGN were $x = -2.13$ mm, $y = -2.07$ mm, $z = -2.75$ mm if the distance between bregma and lambda was 4.2 mm for a mouse. If the distance was not 4.2 mm, the coordinates for the injection

site were calculated proportionally. Cranial drill was used to thin the skull. Glass pipette filled with dyes was inserted to the injection site. In total, 10 × 2.3 nL (one injection every 6 s) CTB-555 was injected into the dLGN. The pipette was pulled out slowly 10 min after injection. Of note, 48 h later, mice were perfused and brains were fixed with 4% PFA, sliced on vibratome machine (Leica, VT 1000S) at 100 μm.

Procedures for the stereotaxic injection of the Adeno-associated virus (AAV) virus into the dLGN were the same as described previously. In total, 200 nL of AAV-syn-GCaMP6 virus was injected into dLGN. Three weeks after injection, mice were perfused with 4% PFA and immnostained with green fluorescent protein (GFP) antibody to visualize axonal projections from dLGN neurons.

Ca^{2+} Imaging In Vivo

In all, 1 μL AAV-syn-GCaMP6 virus was injected intravitreously in *Tra2β*$^{fl/+}$; *Emx1-Cre* and *Tra2β*$^{fl/fl}$; *Emx1-Cre* mice at P0. After recovery for 2 h on 27 °C heating pad (FHC), the pups were put back to their home cage. GCaMP6 was expressed in the axon terminals of RGCs 12–13 days after viral injection surgery. Before the imaging experiment, mice were anesthetized with isoflurane and craniotomy was made right above the SC. Dura was carefully torn off using sharp tweezers and proper amount of warm agarose was added over the craniotomy. A 5-mm diameter glass coverslip (World Precise Instrument Company) was placed onto the craniotomy. The coverslip was further sealed by transparent QWIK-SIL (World Precise Instrument Company). After the surgery, isoflurane was turned off. A series of time-lapse fluorescent images were captured using 2-photon microscope with Mai Tai DeepSee femtosecond pulsed laser at 940 nm through 25× water immersion objective (NA = 1.05, Olympus). Images were collected at about 2–3 Hz (512 × 512 pixels).

All images were analyzed in custom programs written in Matlab. We chose regions of interest (ROIs) manually (Fig. 6*E*,*F* white dotted rectangle inset). Changes in fluorescent signals were averaged within each ROI. A custom software routine written in Matlab calculated the threshold for wave-like activities from the fluorescent signals and automatically detected the onset of these waves (Fig. 6*G*–*I*). Each movie lasted for at least 300 s, and the frequency of retinal waves could be calculated in each ROI. We analyzed several ROIs in each mouse and obtained an average number of wave frequency. $\Delta F/F0$ was calculated as $(F-F0)/F0$, where $F0$ is the fluorescence signal averaged from the first 3 frames without any spontaneous activity. A threshold was automatically calculated for each ROI to minimize false-positive signals. The onset time of each spontaneous activity was recorded when the fluorescent signals first crossed the threshold. The frequency of retinal spontaneous activity was then calculated.

NMDA Induced Lesion in Visual Cortex of Fetal Mice

Surgical procedure in pregnant (E16.5) female mice was described previously in "Embryonic intravitreous injection and analysis of retinal projections." We injected about 50 nL N-methyl-d-aspartic acid (NMDA, Sigma-Aldrich, M3262) at 5 mg/ml in HEPES into the V1 of fetal mice. After recovery from the anesthesia, the pregnant female was put back to the home cage. The pups were intravitreously injected CTB-488 and 555 at P11 and P30 and perfused 48 h later. Coronal sections of the dLGN were collected and imaged as described before.

Cell Counting

Red, Green, Blue images were first converted to 8-bit gray-scale format in ImageJ. ROI was selected using freehand selection tool. The images were inverted to protrude RGC cells. Threshold value of images was adjusted to sharpen the outlines of the cells. The images became binary with only 2 intensities, black 0 and white 255. In order to separate overlapping cells (a common situation in most images), process-binary-watershed procedure was carried out. Finally, size parameter was set from 10 to 10 000 and circularity from 0 to 1 in ImageJ. After all these procedures, the cell number was calculated automatically in ImageJ.

Behavioral Experiment

Metal head bars were implanted onto the skull of mice about 2 months old. The training began after water restriction for 2 days. Static gratings with 0° and 90° orientation were generated by Psychopy2 software at grating size of spatial frequency of 9 cycle/degree. Each grating appeared for 1 s followed by 9 s gray screen. The behavioral experiment was consisted of 3 training session followed by 1 test session. In each training session, 40 gratings were presented, water reward was provided when gratings were at 0°, and no water reward was provided when gratings were at 90°. Eight gratings stimuli were presented in the test session with no water reward. The behavioral responses of the mice in the test session were categorized into 4 groups: correct lick (CL), miss (M), correct reject (CR), and false lick (FL). The experiment lasted for 21 days for each mouse. Fraction of different responses was calculated from 9 to 21 days.

TUNEL Staining

The protocol for the brain slice preparation was the same as described in "Immunohistochemistry." TUNEL staining kit (*In Situ* Cell Death Detection Kit, TMR red, Roche, Cat. No. 12156792910) was used in the staining. Briefly, brain slices were further fixed in 4% PFA for 20 min at room temperature, washed with PBS twice for 30 min. We then added fresh permeabilisation solution (0.1% Triton-X-100, 0.1% sodium citrate) to the slices for 2–3 min on ice. Of note, 300 μL staining reaction solution was added to each slice (reaction solution: 50 μL enzyme solution in 450 μL label solution). Negative control slices were processed at the same time by adding 300 μL label solution only. Slice covered with reaction solution was kept in the incubator at 37 °C for 60 min. After incubation, the slices were washed twice in PBS and observed.

Code Availability

The computer codes in Matlab (Mathworks Inc.) are available. Please send a request to the corresponding author.

Results

Retinal Targeting Defect to the dLGN Starts Around E18.5 in Tra2β cKO Mice

A previous study demonstrated that *Tra2β* cKO mice, generated by inter-crossing of *Tra2β*$^{fl/+}$; *Emx1-Cre* mice, have major cortex loss at P0 (Roberts et al. 2014). Compared with control mice, *Tra2β* cKO mice lack about 85% of the neocortex, with major loss in the caudal and medial parts of the cortex at E16.5 (Fig. 1*A*,*C*). Some parts of the rostral and lateral cortex

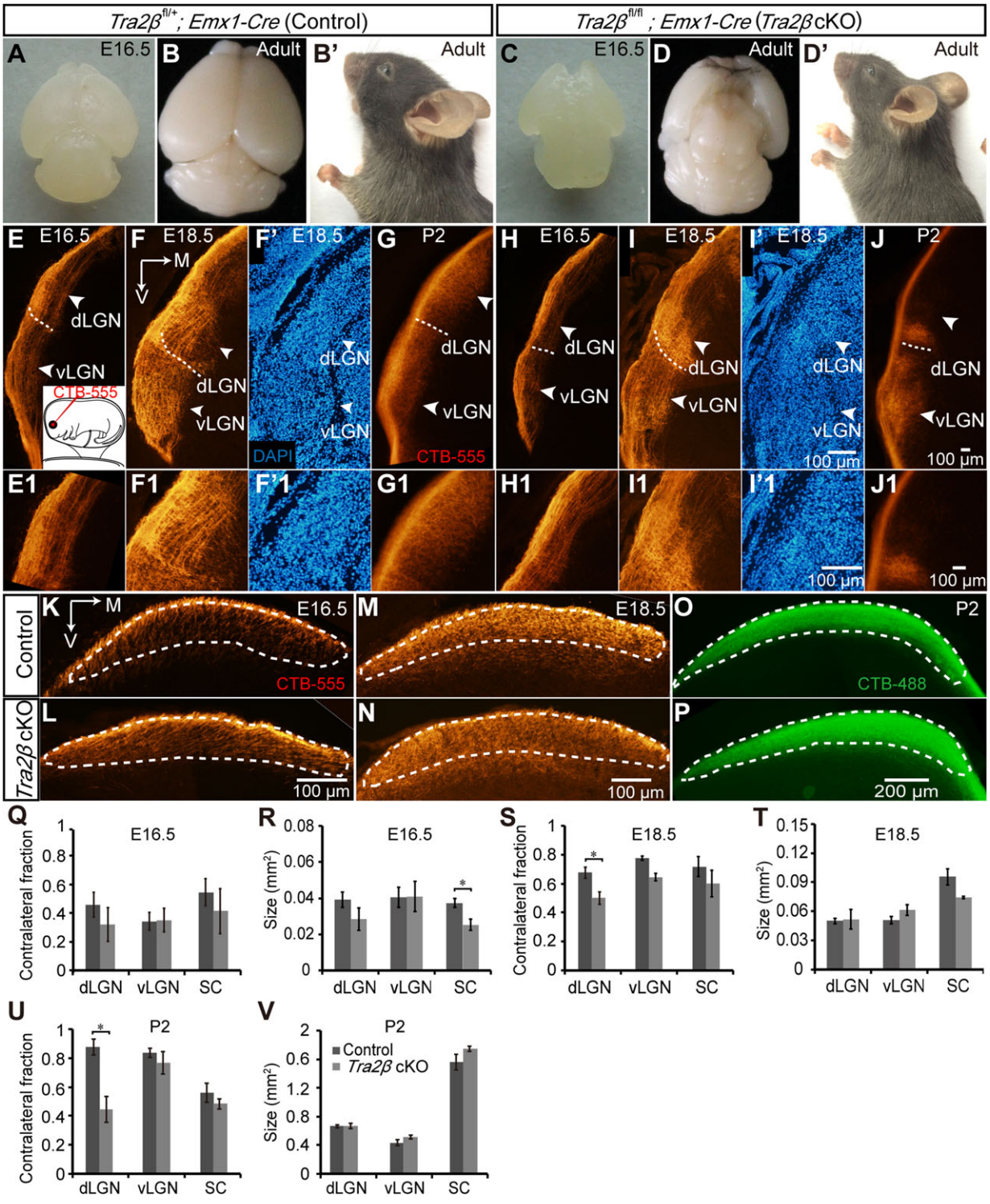

Figure 1. Retinogeniculate and retinocollicular projections in control and *Tra2β* cKO mice by monocular injection of CTB-555. (*A–B*, *C–D*), Whole-mount brain structure of control (*Tra2β*$^{fl/+}$; *Emx1-Cre*) and *Tra2β* cKO (*Tra2β*$^{fl/fl}$; *Emx1-Cre*) mice at E16.5 and adulthood. (*B′,D′*) Sagittal view for the head of control and *Tra2β* cKO mice. (*E–G*) Retinal projections to the LGN at E16.5, E18.5, and P2 in control mice. Schematic of embryonic intravitreous injection was embedded in *E*. (*F′*) DAPI staining showed the territories of the dLGN and vLGN at E18.5 in control mice. The dashed lines showed the ventral border of dLGN. (*E1–G1*) Zoomed-in figures of dLGN corresponded to *E–G*. (*H–J*) Retinal projections to the LGN at E16.5, E18.5, and P2 in *Tra2β* cKO mice. (*I′*) DAPI staining showed the territories of the dLGN and vLGN at E18.5 in Tra2*β* cKO mice. (*H1–J1*) Zoomed-in figures of dLGN corresponded to *H–J*. (*K–P*) Retinal projections to the SC in control and *Tra2β* cKO mice at E16.5 (*K*,*L*), E18.5 (*M*,*N*), and P2 (*O*,*P*). The SC was outlined with white dashed lines. M, medial; V, ventral. (*Q*) Fraction of contralateral projections within the dLGN, vLGN, and SC at E16.5 in control and *Tra2β* cKO mice. (*R*) Sizes of the dLGN, vLGN, and SC at E16.5 in control and *Tra2β* cKO mice (size of SC, $P = 0.037$, $n_{control} = n_{Tra2\beta\ cKO} = 3$, Student's *t*-test). (*S*) Fraction of contralateral projections within the dLGN, vLGN, and SC at E18.5 (Contra fraction within dLGN, $P = 0.044$, $n_{control} = n_{Tra2\beta\ cKO} = 3$, Student's *t*-test). (*T*) Sizes of the dLGN, vLGN, and SC at E18.5 in control and *Tra2β* cKO mice. (*U*) Fraction of contralateral projections within the dLGN, vLGN, and SC at P2 in control and *Tra2β* cKO mice (Contra fraction within dLGN, $P = 0.003$, $n_{control} = n_{Tra2\beta\ cKO} = 5$, Student's *t*-test). (*V*) Sizes of the dLGN, vLGN, and SC at P2 in control and *Tra2β* cKO mice. Bars represented mean ± SEM.

remained at E16.5 and lasted into adulthood (Fig. 1B,D). Despite this remarkable defect in the neocortex, the *Tra2β* cKO mice survived into adulthood and are physically and behaviorally similar to control mice ($Tra2\beta^{fl/+}$; *Emx1-Cre*), except for a smaller and invaginated head (Fig. 1B′,D′). Adult *Tra2β* cKO mice were generally more active than littermates. These results demonstrated that the developmental defect in *Tra2β* cKO mice emerged as early as during late embryogenesis, but did not have a drastic impact on the long-term physical growth.

To determine the time point for the emergence of the retinogeniculate projection defect in *Tra2β* cKO mice, monocular whole eye injection experiments were conducted in fetus and neonatal mice. We analyzed the retinal projections of mouse embryos whose entire retina was uniformly labeled with fluorescent dyes. At E15.5, most of the retinal projections grew along the lateral side of vLGN and dLGN toward medial pretectal nucleus in non-branched axon bundle. At E16.5, while some retinal axons in control mice began to branch in lateral–medial direction in the dLGN (Fig. 1E,E1), fewer axons in *Tra2β* cKO mice branched in lateral–medial direction (Fig. 1H,H1). The density and distribution of axons in the vLGN of control mice were similar to those in *Tra2β* cKO mice (Fig. 1E,H).

By E18.5, the differences in axon arborization between control and *Tra2β* cKO mice were more apparent in the dLGN (Fig. 1F,I,F1,I1). In control mice, the arborization of retinal axons in medial dLGN at E18.5 was much denser compared with that in E16.5 (Fig. 1E1,F1). Axons almost filled the entire territory of the dLGN. However, in *Tra2β* cKO mice, retinal axons failed to fill the territory of the dLGN (Fig. 1I,I1). A majority of the retinal axons were restricted to the ventrolateral corner of the dLGN. The phenotype of retinogeniclate projection defect in *Tra2β* cKO mice lasted to adulthood (Fig. 1G,J,G1,J1, Supplementary Fig. 1). In contrast, retinal projections to the vLGN and other retinal targets were completely normal at E16.5, E18.5, P2, and adulthood (Fig. 1E–J, Supplementary Fig. 2).

We also examined the morphology of the dLGN. DAPI staining clearly exhibited the existence of dLGN structure in *Tra2β* cKO mice (Fig. 1F′,I′,F′1,I′1). Transcription factor FOXP2, which is expressed in visual relays and areas of visual processing (French and Fisher, 2014), shared similar expression profile as control but with lower expression level within the dLGN territory (Supplementary Fig. 3). We next examined the morphology of the dLGN in adulthood. VGLUT2 and serotonin transporter immunostaining showed normal morphology of dLGN in *Tra2β* cKO mice (Supplementary Fig. 3). These data illustrated a relative normal dLGN in *Tra2β* cKO mice.

To quantify the retinal projection defect in the dLGN, we analyzed the amount of axons in the territories of the dLGN, vLGN, and SC. There was no significant difference in the fraction of contralateral projections and the sizes of the dLGN at E16.5 (Fig. 1Q,R). The fraction of contralateral projections in the dLGN of *Tra2β* cKO mice at E18.5 and P2 was significantly smaller than that of control mice (Fig. 1S,U), while the sizes of the dLGN were similar (Fig. 1T,V). Retinal projections to the vLGN were normal (Fig. 1Q–V). We also examined the development of retinal targeting to the SC at E16.5, E18.5, and P2 (Fig. 1K–P). Compared with the fraction of contralateral projections and size of the SC in control mice, those in *Tra2β* cKO mice were significantly smaller at E16.5 but were largely normal at E18.5 and P2 (Fig. 1Q–V). Results in adulthood were similar to those at embryonic stage (Supplementary Fig. 1). In summary, there was a severe decrease in the amount of retinal axons in the dLGN but not vLGN or SC at E18.5 and P2 in *Tra2β* cKO "cortexless" mice.

Expressions of TRA2β in the LGN, Retina, and SC are Normal

It was recently shown that morphological and histological features of the *Tra2β* cKO thalamus are similar to those of control mice (Shanks et al. 2016). To rule out the possibility that the retinal projection defect in the dLGN was due to the disruption of TRA2β expression in the dLGN or retina, we examined the expression of CRE in *Emx1-Cre* mice and TRA2β in *Tra2β* cKO mice. We used *Ai14*; *Emx1*-Cre mice to visualize the expression of Cre recombinase at E16.5 and P1. We found a massive expression of CRE in the neocortex and hippocampus from E16.5 to P1, while there was very sparse CRE expression in both the dLGN and vLGN (Fig. 2A–B′). DAPI staining was used to define the LGN (Fig. 2A′,B′,C′,D′). The expression of TRA2β was similar in the dLGN and vLGN in control and *Tra2β* cKO mice at E18.5 (Fig. 2C–D′) (Hofmann and Wirth, 2002). Further, CRE was not expressed in the retina at E16.5 and E18.5 (Fig. 2E,F). TRA2β signal in the retina was similar in both control and *Tra2β* cKO mice (Fig. 2G,H). DAPI staining showed that the lamination of retina at E16.5 was normal (Fig. 2G′,H′).

CRE was not expressed in the SC in Ai14; *Emx1*-Cre mice at E16.5 (Fig. 2I–J′). The expression of TRA2β in the SC was similar in control and *Tra2β* cKO mice at E16.5 and E18.5 (Fig. 2K–L′). In summary, these results demonstrated that CRE was highly expressed in the cortex and hippocampus but not in the dLGN, vLGN, retina, and SC before P1. Therefore, the retinal projection defect in the dLGN was not likely due to non-selective deletion of TRA2β in *Tra2β* cKO mice.

Apoptosis in dLGN Cells and Thalamocortical Projections in *Tra2β* cKO Mice Before Birth

It was previously reported that there is severe apoptosis in cortical layers at E14.5 and E15.5 but not at later stages of development in *Tra2β* cKO mice (Storbeck et al. 2014). To examine the possible impact of the loss of cortical neurons on the visual circuit, we examined the survival of dLGN, vLGN, and SC neurons at E16.5, E18.5, and P5 in *Tra2β* cKO mice using the apoptosis marker cleaved caspase-3 and TUNEL staining. DAPI staining or retinal CTB intravitreous injection helped to determine the territories of the LGN (data not shown) and SC in control and *Tra2β* cKO mice. There was no expression of cleaved caspase-3 along the thalamocortical pathway or neurons in the dLGN in control mice at E16.5, E18.5, and P5 (Fig. 3A–A′,C–C′,E–E′). Meanwhile, there was no signal in TUNEL staining (Fig. 3A″,C″,E″). In contrast, cleaved caspase-3 expression was observed in the dLGN neurons and along the thalamocortical pathway at E16.5, with almost no expression in the vLGN of *Tra2β* cKO mice (Fig. 3B–B″). A small amount of dLGN neurons as well as the thalamocortical pathway expressed cleaved caspase-3 at E18.5, with no expression in the vLGN (Fig. 3D–D′). In accordance with the cleaved caspase-3 staining results, TUNEL staining showed late-stage apoptosis in dLGN cells at E16.5 and E18.5 (Fig. 3B″,D″). At P5, neither cleaved caspase-3 expression nor TUNEL staining signal was detected in both dLGN and vLGN of *Tra2β* cKO mice (Fig. 3F–F″). Meanwhile, cleaved caspase-3 was not expressed in the SC at E16.5, E18.5, or P5 in either control or *Tra2β* cKO mice (Fig. 3G–L′). These results indicated that a small fraction of dLGN neurons went through apoptosis at around E16.5, but left the gross morphology of dLGN spared in *Tra2β* cKO mice (Fig. 3B″,D″).

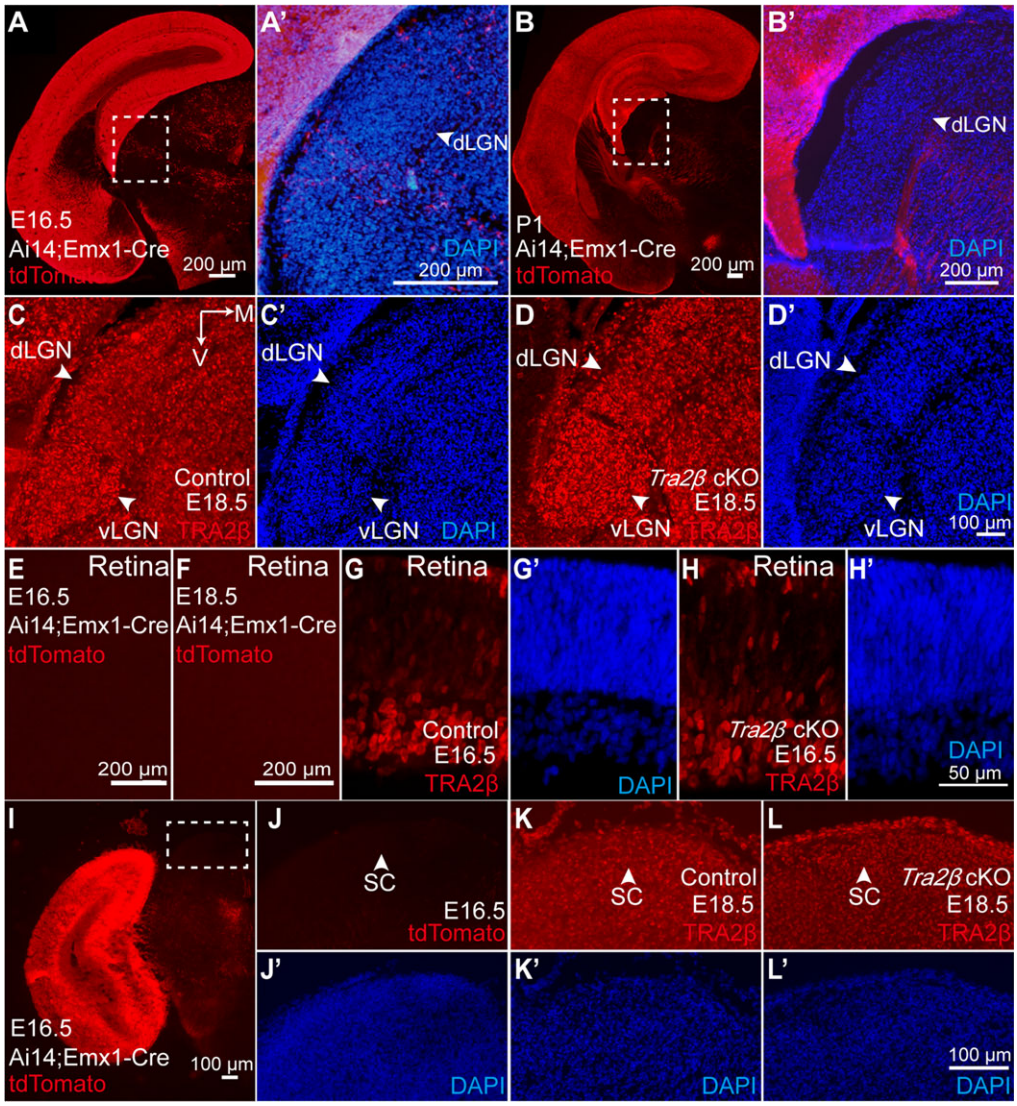

Figure 2. Expression of Cre and TRA2β in control and *Tra2β* cKO mice. (*A*) Expression of CRE-tdTomato at E16.5 in the cortex and LGN in Ai14; *Emx1*-Cre mice. (*A′*) High magnification image of the inset area in *A*. (*B*) Expression of CRE-tdTomato at P1 in the cortex and LGN. (*B′*) High magnification image of the inset area in *B*. (*C*,*D*) Expression of TRA2β in the LGN of control and *Tra2β* cKO mice at E18.5. (*C′*,*D′*) DAPI staining helped to define the territory of LGN corresponding to *C* and *D*. (*E*,*F*) Expression of CRE-tdTomato in the whole-mount retina of Ai14; *Emx1*-Cre mice at E16.5 and E18.5, respectively. (*G*) Expression of TRA2β in the sliced retina of control mice at E16.5. (*G′*) DAPI staining to show the lamination of retina in *G*. (*H*) Expression of TRA2β in the sliced retina of *Tra2β* cKO mice at E16.5. (*H′*) DAPI staining to show the lamination of retina in *H*. (*I*) Expression of CRE-tdTomato at E16.5 in SC. (*J*) High magnification image of the inset area in *I*. (*J′*) DAPI staining to show the territory of the SC in *J*. (*K*,*L*) Expression of TRA2β in the SC of control and *Tra2β* cKO mice at E18.5. (*K′*,*L′*) DAPI staining helped to define the territory of the SC corresponding to *K* and *L*.

No Light Response in the dLGN of *Tra2β* cKO Mice

Defects of retinal projections to the dLGN in *Tra2β* cKO mice suggested that dLGN is no longer a functional part of the visual circuit. We examined the light response of the dLGN by stereotaxically inserting a single electrode into the dLGN of control and *Tra2β* cKO mice (Fig. 4*A*–*B*,*E*). Light response from the dLGN of *Tra2β* cKO mice was sparse during the 1-s whole-field light stimulation, while a large number of spikes were evoked during light stimulation in control mice (Fig. 4*C*,*D*,*F*–*H*). After *in vivo* electrophysiological experiments, brains were dissected and bright-field or fluorescence images showed positions of the electrodes and the shape of the dLGN (Fig. 4*B*,*E*). These results confirmed the fact that retinal projections to the dLGN were mostly absent in *Tra2β* cKO mice.

Disrupted Projections Between the dLGN and V1 in *Tra2β* cKO Mice

Previous experiments (Roberts et al. 2014) and our results have demonstrated that a majority of cortex was absent in *Tra2β* cKO mice. To confirm that the dLGN did not receive exogenous projections from the remaining cortical areas, we first conducted retrograde labeling experiments by injecting CTB-555 dyes into the dLGN or SC in adult control and *Tra2β* cKO mice (Fig. 5*A*–*D*). A great number of neurons were labeled in layer VI in the visual cortex of control mice (Fig. 5*A′*). In contrast, no cell body was detected in the remaining cortex of *Tra2β* cKO (Fig. 5*B′*), indicating that the normally massive feedback connections between visual cortex and dLGN were missing in *Tra2β* cKO mice. Visual cortex also normally sends direct projections to SC

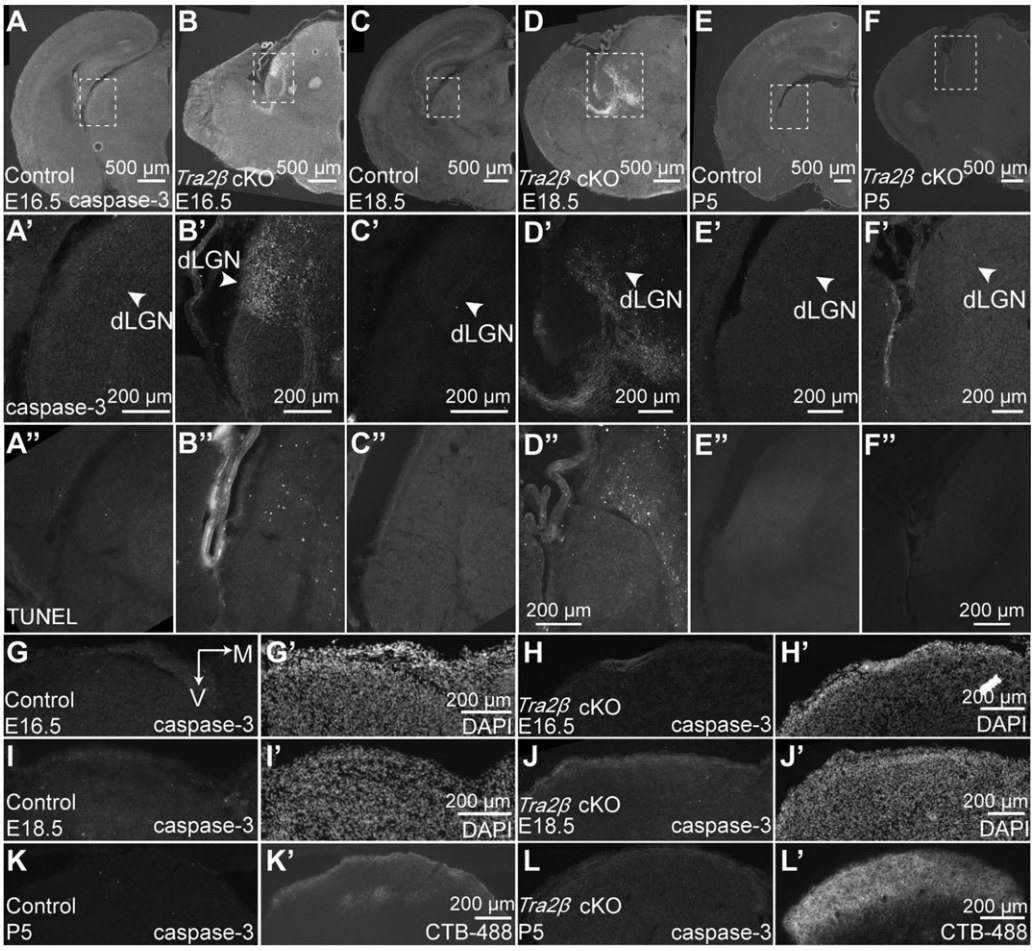

Figure 3. Apoptosis in the dLGN cells and thalamocortical pathway in *Tra2β* cKO mice. (*A–B″*) Immunohistochemistry for cleaved caspase-3 and TUNEL staining at E16.5 in the cortex and dLGN of control and *Tra2β* cKO mice respectively. (*C–D″*) Immunohistochemistry for cleaved caspase-3 and TUNEL staining at E18.5 in the cortex and dLGN of control and *Tra2β* cKO mice. (*E–F″*) Immunohistochemistry for cleaved caspase-3 and TUNEL staining at P5 in the cortex and dLGN of control and *Tra2β* cKO mice. (*A′–F′*) High magnification images of the areas labeled by white dotted lines in *A–F*, respectively. (*G–L′*) Immunohistochemistry for cleaved caspase-3 and DAPI staining or CTB labeling at E16.5, E18.5, and P5, respectively, in SC of control and *Tra2β* cKO mice.

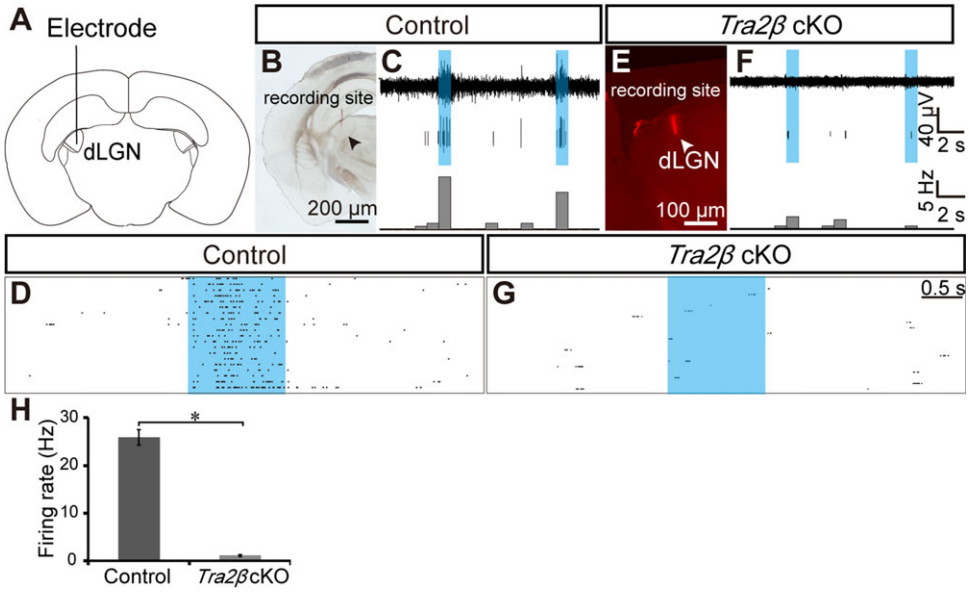

Figure 4. Light responses in the dLGN of adult *Tra2β* cKO mice. (*A*) Schematic of electrophysiological recording in dLGN. (*B,E*) Recording sites labeled by DiI in dLGN of control and *Tra2β* cKO mice, respectively. (*C,F*) Examples of light responses in the dLGN of control and *Tra2β* cKO mice, respectively (top: raw data; middle: raster plots for spikes; bottom: firing rates). Blue shadows represented light stimulation. (*D,G*) Raster plots showing spike activities during light stimulation in control and *Tra2β* cKO mice. (*H*) The average firing rates in the dLGN of control and *Tra2β* cKO mice during light stimulation ($P = 0.0001$, $n_{control} = n_{Tra2\beta\ cKO} = 3$, Student's *t*-test).

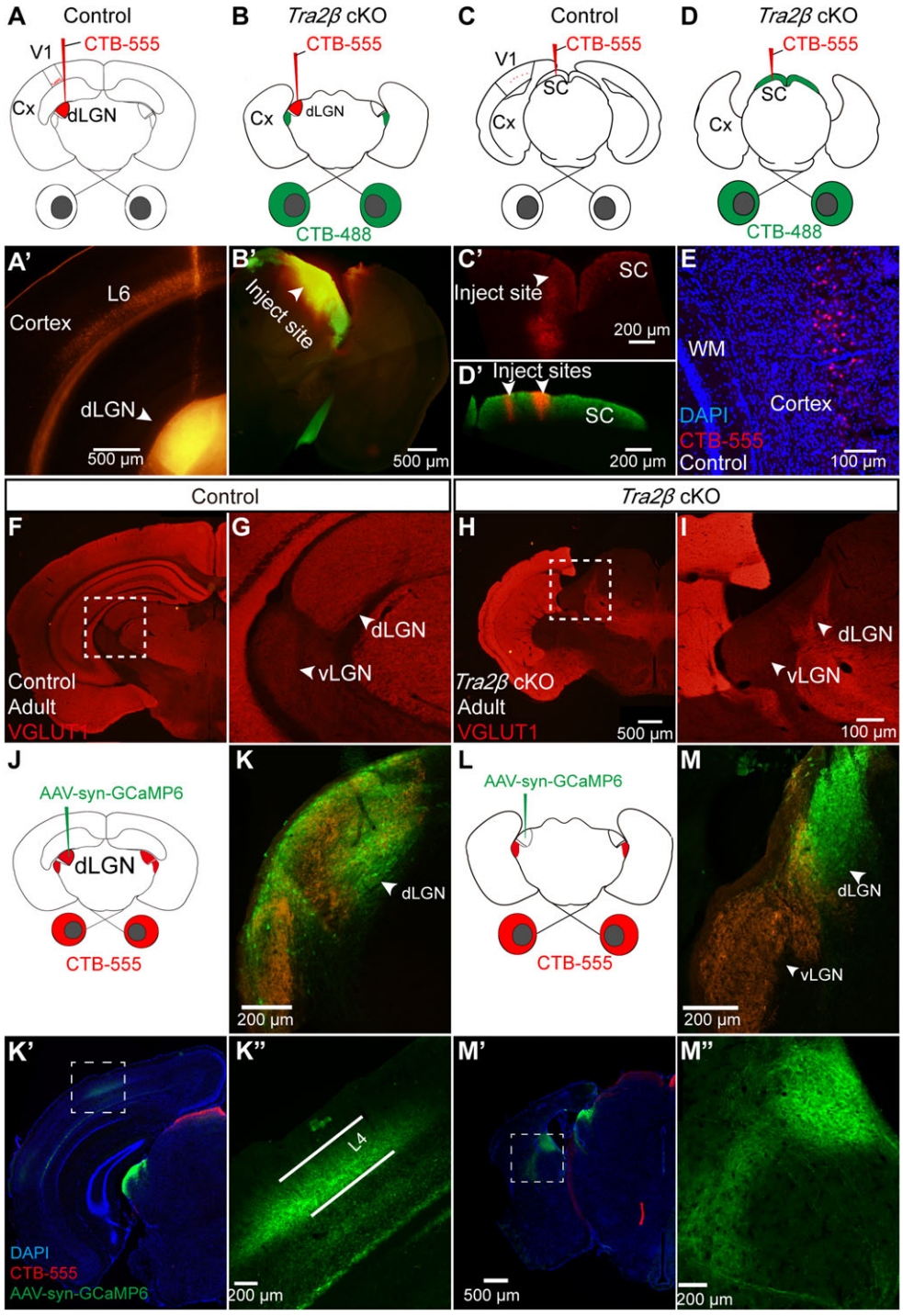

Figure 5. The absence of corticogeniculate feedback projections in *Tra2β* cKO mice. (*A–D*) Schematics of the stereotaxic injections into the dLGN and SC of control and *Tra2β* cKO mice to retrogradely label thalamic projecting neurons. Cx: Cortex. (*A′*) Retrogradely labeled cells in layer VI of cortex after CTB-555 injection into dLGN in adult control mice. (*B′*) No cells were labeled in the cortex after CTB-555 injection into the dLGN in adult *Tra2β* cKO mice. CTB-488 eye injections help to show the position of the dLGN. (*C′*) The injection site of CTB-555 in the SC in adult control mice. (*D′*) Two injection sites of CTB-555 in the SC in adult *Tra2β* cKO mice. (*E*) Retrogradely labeled cells in the cortex after CTB-555 injection into SC in control mice. WM, white matter. (*F,G*) Immunohistochemistry for VGLUT1 in adult control mice. (*G*) A higher magnification image of the inset in *F*. (*H,I*) Immunohistochemistry for VGLUT1 in adult *Tra2β* cKO mice. (*J*) Schematics of the stereotaxic dLGN injection experiment in adult control mice. (*K*) Expression of GCaMP6 in the dLGN neurons. (*K′*) Low magnification image showed the projection from the dLGN to the cortex. (*K″*) High magnification image to show details of the inset in *K′*. (*L*) Schematics of the stereotaxic dLGN injection experiment in adult *Tra2β* cKO mice. (*M*) Expression of GCaMP6 in the dLGN neurons. (*M′*) dLGN axons in *Tra2β* cKO mice. (*M″*) High magnification image to show details of the inset in *M′*.

(Fries 1985; Wang and Burkhalter 2013). We next examined the corticocollicular feedback projections by injecting CTB-555 dye into the SC. Again, a small number of retrogradely labeled neurons existed in the cortex in control mice (Fig. 5*C′*,*E*), but no cells were visible in the remaining cortex of *Tra2β* cKO mice (Fig. 5*D′*), which indicates the loss of cortical feedback projections to both the dLGN and SC.

To further rule out the possibility that the functions of the lost visual cortical neurons were compensated for by remaining cells, we examined the expression of VGLUT1, which is the main transporter in the axon terminals of corticogeniculate feedback projections (Fujiyama et al. 2003; Nakamura et al. 2005). VGLUT1 immunofluorescence signals existed in the entire dLGN but not vLGN in control mice (Fig. 5F,G), verifying the specificity for VGLUT1 to label corticogeniculate terminals from layer VI. However, no VGLUT1 signals were detected in the dLGN in *Tra2β* cKO mice (Fig. 5H,I), demonstrating that there were no functional feedback connections between layer VI cortex and the dLGN in *Tra2β* cKO mice. In summary, these results collectively demonstrated that the structural and functional feedback connections from the cortex to the dLGN are absent in *Tra2β* cKO mice.

Because the structure of the dLGN was largely intact, we further investigated the projection from the dLGN in *Tra2β* cKO mice. AAV-syn-GCaMP6 virus was stereotaxically injected into the dLGN to label axons originating from dLGN neurons in control and *Tra2β* cKO mice (Fig. 5J,L). Retinal axons labeled by CTB-555 in the dLGN verified that AAV was successfully injected into the dLGN (Fig. 5K,M). In control mice, dLGN axon terminals mostly distributed in layer IV of V1 (Fig. 5K′,K″). In *Tra2β* cKO mice, dLGN projection neurons did not target the cortex but instead projected to a restricted territory outside the remaining cortex (Fig. 5M′,M″). These results collectively demonstrated that neurons in the dLGN send projections to a non-cortical area and receive no feedback input from the cortex in *Tra2β* cKO mice.

Retinal Morphology and Spontaneous Activity is Normal in *Tra2β* cKO Mice

Previous studies demonstrated that spontaneous retinal waves play a critical role in the development of retinofugal projections in mice during the first 2 postnatal weeks (Huberman et al. 2008; Feller, 2009; Zhang et al. 2012; Denman and Contreras, 2015). DAPI staining indicated that retinal structure was normal in *Tra2β* cKO mice (Fig. 6A–A′). The number of Brn3a labeled cells was similar in *Tra2β* cKO and control mice (Supplementary Fig. 4). These results showed that *Tra2β* conditional deletion did not induce either apoptosis or over proliferation in RGCs. Former reports have confirmed that retinal waves propagated throughout the visual system and can be visualized in the SC or visual cortex in awake-behaving mice (Ackman et al. 2012). Unlike control mice in which only a small amount of medial and posterior SC is exposed, SC was completely uncovered in *Tra2β* cKO mice due to the major loss of medial to posterior neocortex and the hippocampus (Fig. 1D). Moreover, our previous results showed that retinal projections to the SC were normal in *Tra2β* cKO mice (Fig. 1L,N,P). We therefore measured retinal waves by *in vivo* 2-photon Ca^{2+} imaging of retinal axons

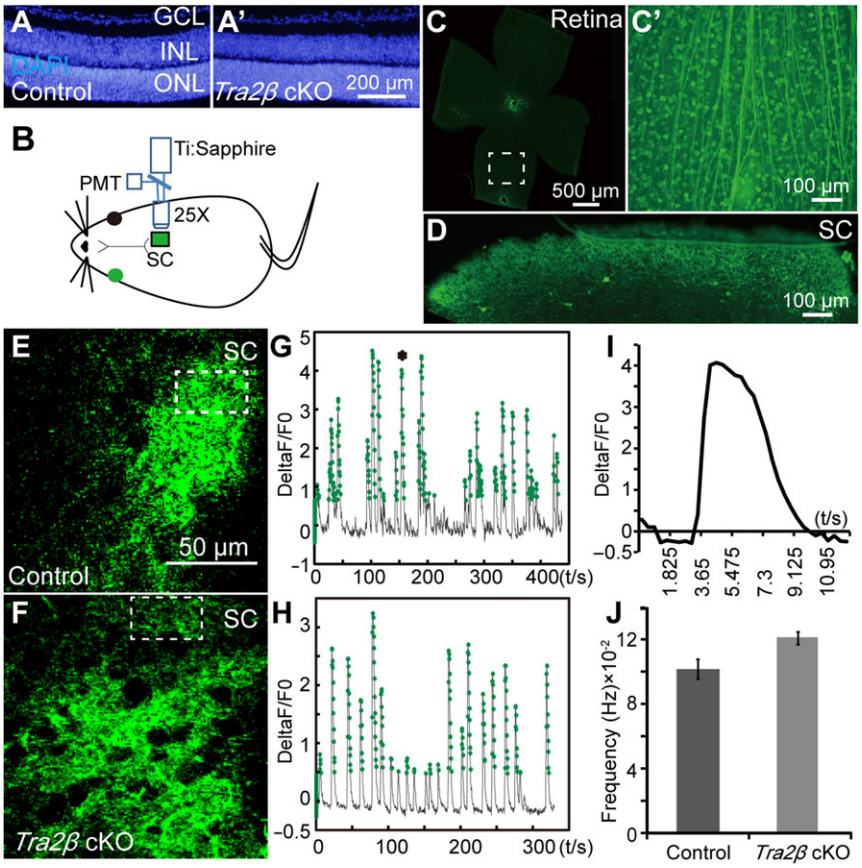

Figure 6. Retinal morphology and waves in awake-behaving *Tra2β* cKO mice. (A–A′) Retina structure of control and *Tra2β* cKO mice. GCL: ganglion cell layer, INL: inner nucleus layer, ONL: outer nucleus layer. (B) Schematic of Ca^{2+} imaging experiment. (C) Expression of GCaMP6 in the whole-mount retina. (C′) High magnification image of the inset area in C. (D) Expression of GCaMP6 in axon terminals of RGCs in the SC. (E,F) GCaMP6 fluorescent signals from axon terminals in awake control and *Tra2β* cKO mice. (G,H) Changes of fluorescent signals in the white rectangular area in E and F, respectively. One peak represented the event of one retinal wave. (I) One typical retinal wave labeled by asterisk in G. (J) Average frequency for retinal waves in control and *Tra2β* cKO mice. Bars represented mean ± SEM.

terminals in SC. We injected AAV-syn-GCaMP6 virus into retinas of control and *Tra2β* cKO mice at P1. Imaging experiments conducted after the expression of GCaMP6 stabilized at P12 (Fig. 6*B*). To make sure that all mice used in imaging experiments had sufficient virus infection efficiency, we performed immunohistochemistry staining for GCaMP6 after each experiment. Most RGCs expressed GCaMP6 and were clearly visible (Fig. 6*C*–*C*′), and their axonal terminals that expressed GCaMP6 distributed throughout the superficial layer of SC (Fig. 6*D*). These results ensured the reliability of Ca^{2+} signals detected in SC. Two example frames from the movies of fluorescent changes in control and *Tra2β* cKO mice were shown (Fig. 6*E*,*F*). ROIs were selected manually. One peak in the calcium signals indicated one retinal wave (Fig. 6*G*,*H*). An individual retinal wave labeled by black asterisk in Figure 6*G* was shown (Fig. 6*I*). There was no significant difference in the average frequency of retinal waves between control and *Tra2β* cKO mice (Fig. 6*J*).

Prenatal Visual Cortex Lesion Disrupted the Retinogeniculate Projection

To confirm that the absence of corticothalamic connections could lead to the abnormal retinogeniculate projections, we conducted pharmacological visual cortex lesion using NMDA (Beal et al. 1991; Caleo et al. 2002; Kim et al. 2006) at E16.5 (Fig. 7*A*–*A*′). Retinogeniculate projections in the lesioned mice were severely disturbed at P13 and P32 in the hemisphere ipsilateral to the lesion (Fig. 7*F*–*H*″). A majority of the contralateral retinogeniculate projections disappeared (Fig. 7*F*,*H*), which was similar to that in *Tra2β* cKO mice. However, the ipsilateral retinogeniculate projections seemed unaffected in both ages (Fig. 7*F*′,*H*′). As a control of the lesion experiments, retinogeniculate projections (including contralateral, ipsilateral, and overlap fractions) to dLGN in the hemisphere contralateral to the lesion exhibited no defect (Fig. 7*B*–*B*″,*D*–*D*″). However, NMDA lesion of V1 did not affect the eye-specific segregation phenotype of SC on either sides at P13 and p32 (Fig. 7*C*–*E*″,*G*–*I*″).

To examine the role of corticogeniculate connections in the development of retinal projections, we utilized *Fezf2* cKO mice whose corticogeniculate projections are disrupted from embryonic stages (Han et al. 2011). In order to visualize corticogeniculate feedback projections, *Fezf2*-floxed mice were bred with both CAG-*Cat*-*Gfp* and *Emx1*-*Cre* mice. The corticogeniculate feedback projections (*Emx1*-*Cre*; CAG-*Cat*-*Gfp*) were markedly reduced in *Fezf2* cKO mice (Fig. 8*A*,*D*), but geniculocortical projections labeled by L1-CAM (Fukuda et al. 1997; López-Bendito et al. 2002) were largely normal in *Fezf2* cKO mice (Supplementary Fig. 5*A*–*F*′). The contralateral retinogeniculate fraction was significantly increased in *Fezf2* cKO mice compared with control mice (Fig. 8*B*,*E*,*G*), while the ipsilateral and overlap fractions were similar (Fig. 8*B*′,*B*″,*E*′,*E*″,*G*). The size of dLGN decreased in *Fezf2* cKO mice compared with that in control mice (Fig. 8*B*,*E*,*H*). Unlike *Tra2β* cKO mice, *Fezf2* cKO mice had very sparse expression of cleaved caspase-3 in the dLGN (Supplementary Fig. 5*G*–*L*′). Retinogeniculate projections to vLGN and SC were similar in control and *Fezf2* cKO mice (Fig. 8*C*–*C*″,*F*–*F*″,*I*,*J*). These results together demonstrate that disrupting corticogeniculate feedback projections can impact developing retinogeniculate projections.

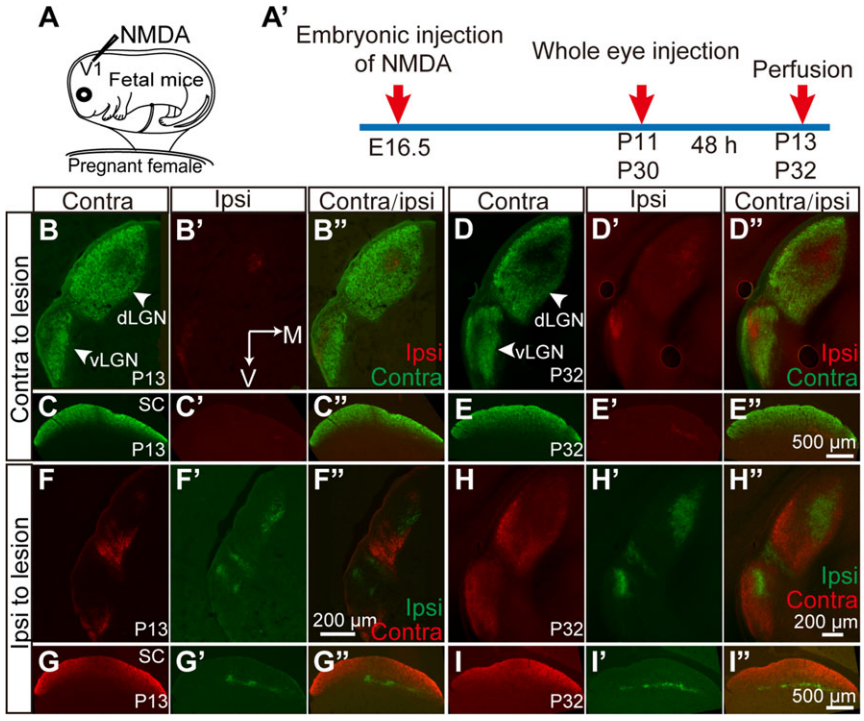

Figure 7. Retinothalamic projections after NMDA induced pharmacological lesion in visual cortex at E16.5. (*A*–*A*′) Schematic of NMDA induced pharmacological lesion experiment in visual cortex. (*B*–*B*″) Eye-specific segregation of dLGN and vLGN in the hemisphere contralateral to lesion at P13 after NMDA injection at E16.5 (*B*: contralateral projections, *B*′: ipsilateral projections, *B*″: overlap projections). (*C*–*C*″) Eye-specific segregation of SC in the hemisphere contralateral to lesion at P13 after NMDA injection at E16.5. (*D*–*D*″) Eye-specific segregation of dLGN and vLGN in the hemisphere contralateral to lesion at P32 after NMDA injection at E16.5. (*E*–*E*″) Eye-specific segregation of SC in the hemisphere contralateral to lesion at P32 after NMDA injection at E16.5. (*F*–*F*″) Eye-specific segregation of dLGN and vLGN in the hemisphere ipsilateral to lesion at P13 after NMDA injection at E16.5. (*G*–*G*″) Eye-specific segregation of SC in the hemisphere ipsilateral to lesion at P13 after NMDA injection at E16.5. (*H*–*H*″) Eye-specific segregation of dLGN and vLGN in the hemisphere ipsilateral to lesion at P32 after NMDA injection at E16.5. (*I*–*I*″) Eye-specific segregation of SC in the hemisphere ipsilateral to lesion at P32 after NMDA injection at E16.5.

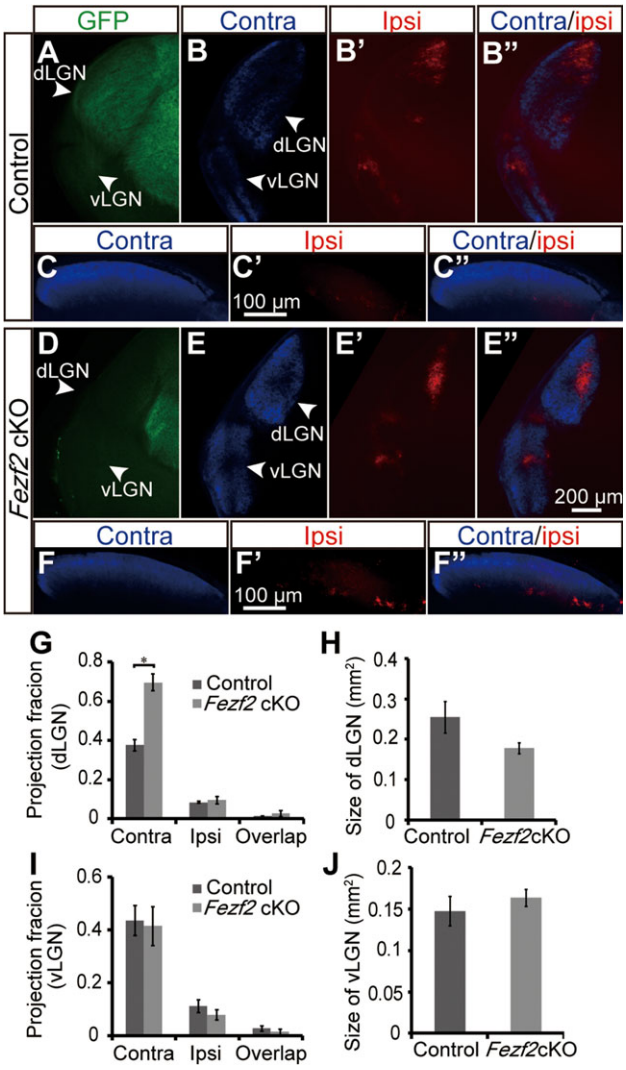

Figure 8. Retinogeniculate projections disrupted in *Fezf2* cKO mice. (*A*) corticogeniculate projections visualized by GFP in control (*Fezf2*$^{fl/+}$; *Emx1-Cre*; *Cat-GFP*) mice at P13. (*B–B″*) Eye-specific segregation of the dLGN and vLGN in control mice at P13 (*B*: contralateral projections, *B′*: ipsilateral projections, *B″*: overlap projections). (*C–C″*) Eye-specific segregation of the SC in control mice (*C*: contralateral projections, *C′*: ipsilateral projections, *C″*: overlap projections). (*D*) Corticogeniculate projections visualized by GFP in *Fezf2* cKO (*Fezf2* $^{fl/fl}$; *Emx1-Cre*; *Cat-GFP*) mice at P13. (*E–E″*) Eye-specific segregation of the dLGN and vLGN in *Fezf2* cKO mice at P13. (*F–F″*) Eye-specific segregation of the SC in *Fezf2* cKO mice. (*G,I*) Fractions of contralateral, ipsilateral, and overlap projections in the dLGN and vLGN in control and *Fezf2* cKO mice (fractions of contralateral projections in the dLGN, $P = 0.0136$, $n_{control} = 5$, $n_{Tra2\beta\ cKO} = 3$, Student's *t*-test). (*H,J*) Sizes of the dLGN and vLGN in control and *Fezf2* cKO mice.

Orientation Selectivity was Disrupted in *Tra2β* cKO Mice

It has been shown that even though the major image-forming circuit, namely retinal-dLGN-V1 circuit, was absent, *Tra2β* cKO mice can still perform visual-dependent tasks (Shanks et al. 2016). We next used go-no go experiment to examine whether the orientation selectivity is intact in *Tra2β* cKO mice (Fig. 9A, Supplementary Movies 1 and 2). After being trained for 9 days, control mice can distinguish 0° from 90° orientation with the fraction of CL above 33%. *Tra2β* cKO mice showed significantly lower CL fraction and higher M fraction compared with control mice (Fig. 9B). Meanwhile, there was no significant difference in the fractions of CR and FL between control and *Tra2β* cKO mice (Fig. 9B). We also grouped CL and CR together as correct response and M and FL together as false response. The control mice exhibited a much higher fraction of correct response compared with *Tra2β* cKO mice (Fig. 9C). Together, these data illustrated that orientation selectivity in *Tra2β* cKO mice was weaker than that in control mice.

Discussion

Feedback projections from cortex to subcortical structures such as dLGN and SC are well known to modulate visual responses, but their potential role in the development of primary visual circuit targeting and arborization is unknown. Shanks et al. (2016) showed that cortical input is at least partially required for RGC axons to innervate dLGN but not for arborization in other visual nuclei that do not directly project to the cortex. It was unclear, however, how this effect was mediated, especially in light of evidence that few or no corticothalamic axons are present in or near the dLGN until roughly a week after RGC axons have targeted, branched, and begun elaborating within dLGN, and also that the timing of postnatal corticothalamic axon arborization in the dLGN actually depends on the prior existence of RGC axons (Seabrook et al. 2013). In this study, we showed that the arborization defect was observed at E18.5 in Tra2β cKO mice, implying that something besides corticogeniculate projections is responsible for mediating retinogeniculate axon targeting and branching. Instead, we find that a small population of dLGN neurons undergoes apoptosis at E16.5–E18.5 in Tra2β cKO mice, which better matches the timeline for the failure of RGC-dLGN innervation. Morphology of retinas and spontaneous retinal waves were normal, excluding the possibility that the targeting defect originated from the retina or activity-dependent refinement. Consistent with the results from *Tra2β* cKO mice, retinogeniculate projections were disrupted in both early cortical lesion and *Fezf2* cKO mice that has disrupted cortical input to the dLGN. Meanwhile, Shank et al. also showed a similar retinal projection defect to the dLGN in *Tbr1* KO mice, whose cortical axons fail to target thalamus and instead project to the subcrerbral targets of layer V cortical neurons. These data show some of the first evidence that cortical axons are required for RGC axons to innervate the dLGN.

These findings raise important questions about the mechanism for reciprocal connections to affect the development of retinal axons. Previous studies showed that layer VI cortical axons reached the dorsal thalamus at E18.5 (Hevner et al. 2002) and paused at the medial shell of the dLGN until P2 (Jacobs et al. 2007; Seabrook et al. 2013). The innervation of cortical axons in the dLGN begins at around P4. Shanks et al. (2016) presented a retinal projection phenotype to the dLGN at P2 and proposed a hypothesis that a small number of pioneer axons from the cortex exist in the vicinity of the dLGN, providing a cue for retinal axon arborization and innervation. Alternatively, cortical axons at the medial shell of the dLGN could normally provide either adhesion or growth-promoting cues or cues to remove repellent activity at the dLGN. Potential candidates for such cues include Reelin (Su et al. 2011) and Aggregan (Brooks et al. 2013).

Our results showed that the targeting defect started between E16.5 and E18.5, a time when a great majority of cortical axons have not entered the dLGN. A possibility for the requirement of cortex in retinal axon targeting to the dLGN is that the absence of cortex results in the inability of a cell population in the dLGN to connect with their normal cortical target and affects their survival or differentiation, thus making them unsuitable targets for retinal axons. Previous studies showed

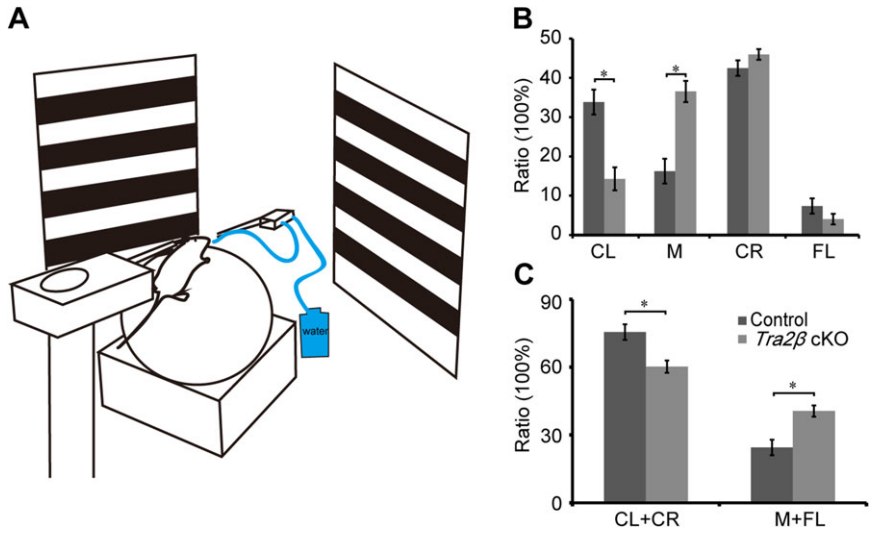

Figure 9. Orientation selectivity in *Tra2β* cKO mice. (*A*) Schematic of the orientation-selective experiment. (*B*) Performance of *Tra2β* cKO and control mice in go-no go experiments. CL, CR, M, and FL (CL: $P = 1.5 \times 10^{-5}$, $n_{control} = 3$, $n_{Tra2\beta cKO} = 3$, Student's *t*-test. CR: $P = 7 \times 10^{-6}$, $n_{control} = 3$, $n_{Tra2\beta\ cKO} = 3$, Student's *t*-test). (*C*) Performance of *Tra2β* cKO and control mice in go-no go experiments with correct (CL + CR) and false (M + FL) responses (correct responses: $P = 2 \times 10^{-4}$, $n_{control} = 3$, $n_{Tra2\beta\ cKO} = 3$, Student's *t*-test; false responses: $P = 6 \times 10^{-5}$, $n_{control} = 3$, $n_{Tra2\beta\ cKO} = 3$, Student's *t*-test).

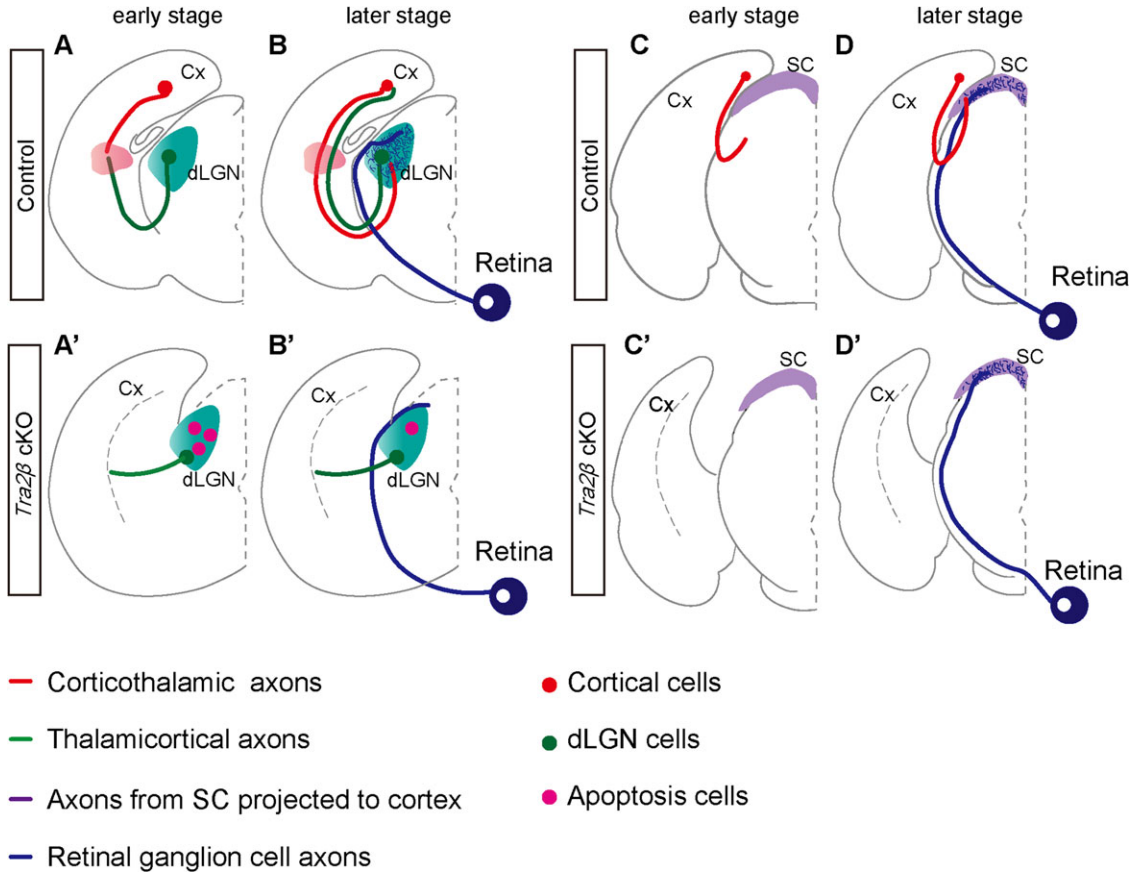

Figure 10. Schematics for the proposed development of retina-dLGN-V1 and retinal-SC circuit. (*A–B*) Development of corticothalamic axons, thalamocortical axons and retinogeniculate projections circuitry during embryonic stages in control mice. (*A'–B'*) Development of corticothalamic axons, thalamocortical axons and retinogeniculate projections circuitry during embryonic stages in *Tra2β* cKO mice. (*C–D*) Development of corticolliculus axons and retinogeniculate projections circuitry during embryonic stages in control mice. (*C'–D'*) Development of corticolliculus axons and retinogeniculate projections circuitry during embryonic stages in *Tra2β* cKO mice.

that thalamic axons navigate toward cortical axons in the subpallium/pallium boundary at E15.5 (Deck et al. 2013), when cortical and thalamic axons interact and guide each other's growth (Hevner et al. 2002; Deck et al. 2013) and that neurons in dorsal thalamus connect to the cortex as early as E18.5 (Hevner et al. 2002). The fact that cleaved caspase-3 is expressed in the

Tra2β cKO mouse dLGN at E16.5 supports the idea that survival of neurons in the dLGN was affected by the absence of cortical connectivity, which may in turn disrupt cues for the wiring of retinal axons. Indeed, the retinal-targeting defect begins around E18.5 in Tra2*β* cKO mice, after the dLGN-specific cell death (at ca. E16.5). Therefore, the mis-targeting of retinal axons may arise from the absence of cues that are normally provided by a fraction of dLGN neurons, or it could be caused by the absence of the dLGN neurons themselves. The morphology of the dLGN is largely normal at E18.5 and TUNEL labeled a handful of cells in the dLGN, indicating that a majority of dLGN cells survived. No cells in the dLGN expressed cleaved caspase-3 at P5, indicating that there may be a specific critical period for thalamocortical connectivity affecting cell survival. The fact that dLGN axons misrouted to an undefined structures outside the remaining cortex in adult *Tra2β* cKO mice also suggested that a large portion of projecting neurons from the dLGN survived until adulthood. We also sought to study the possible reasons for the difference in phenotypes between *Tra2β* cKO and *Fezf2* cKO mice. In Tra2β cKO mice, loss of reciprocal connections between the cortex and thalamus leads to apoptosis in the dLGN neurons and major loss of retinal projections to the dLGN. On the other hand, in Fezf2 cKO mice, neurons in the dLGN still send projections to the cortex despite a major loss in the corticogeniculate projections, which may have spared them from apoptosis. The phenotype in the retinal projections in Fezf2 cKO mice was therefore less severe.

To further elucidate the mechanisms contributing to the cortical guidance of retinal axon targeting, we examined the development of retinal projections to the SC and vLGN. Despite the absence of cortical feedback projections to SC, we did not find any defect in the retinocollicular projections and retinal projections to the vLGN in *Tra2β* cKO mice (Fig. 1*L*,*N*,*P*) and *Fezf2* cKO mice (Fig. 8*E*–*F*″). We showed that cleaved caspase-3 was not expressed in either the SC or vLGN at E16.5 and onwards (Fig. 3*H*,*J*,*L*). Together with the defect in retinal targeting to the dLGN with high expression of cleaved caspase-3 in the dLGN, our results indicated that the survival of some target neurons is crucial for the correct projection of retinal axons, and that RGC decisions to branch and arborize into individual target nuclei are likely independent of each other. Since SC and vLGN neurons do not send axons directly to visual cortex, we propose that cortical input mostly affected the survival of projecting neurons with cortical targets. Our work may thus shed light on a novel scheme for the precise wiring of multiple feedforward and feedback circuits (Fig. 10).

Disruptions of many previously reported factors such as Isl2, and EphrinAs lead to defects in the segregation pattern of binocular input to the dLGN (Pak et al. 2004; Pfeiffenberger et al. 2005). In the *Tra2β* cKO mice, the retinal projection to the dLGN is almost absent, indicating that cortical innervation in early embryonic stage is essential for not only refinement but the targeting of retinal axons to the dLGN. Preliminary results from RNA-seq experiments suggested that transcriptions of previously reported molecules were not significantly different in the dLGN of *Tra2β* cKO mice. However, some other genes were significantly changed in the dLGN of *Tra2β* cKO mice (data not shown).

Funding

National Science Foundation of China (31271158, 31421091, and 31422025 to J.Z.); Science and Technology Commission of Shanghai Municipal (13PJ1401000 to J.Z.); the Young 1000 Plan and Ministry of Science and Technology of the People's Republic of China (2015AA020512 to J.Z.); National Institutes of Health (grants MH105972, MH103339 to N.S. and grants EY023105, EY015788 to M.C.).

Supplementary Material

Supplementary material is available at *Cerebral Cortex* online.

Notes

Conflict of Interest: The authors declare no competing financial interests.

References

Ackman JB, Burbridge TJ, Crair MC. 2012. Retinal waves coordinate patterned activity throughout the developing visual system. Nature. 490:219–225.

Beal MF, Swartz KJ, Finn SF, Mazurek MF, Kowall NW. 1991. Neurochemical characterization of excitotoxin lesions in the cerebral-cortex. J Neurosci. 11:147–158.

Boire D, Théoret H, Herbin M, Casanova C, Ptito M. 2000. Retinogeniculate projections following early cerebral hemispherectomy in the vervet monkey. Exp Brain Res. 135: 373–381.

Briggs F, Usrey WM. 2007. A fast, reciprocal pathway between the lateral geniculate nucleus and visual cortex in the macaque monkey. J Neurosci. 27:5431–5436.

Briggs F, Usrey WM. 2011. Corticogeniculate feedback and visual processing in the primate. J Physiol. 589:33–40.

Brooks JM, Su J, Levy C, Wang JS, Seabrook TA, Guido W, Fox MA. 2013. A molecular mechanism regulating the timing of corticogeniculate innervation. Cell Rep. 5:573–581.

Caleo M, Cenni MC, Costa M, Menna E, Zentilin L, Giadrossi S, Giacca M, Maffei L. 2002. Expression of BCL-2 via adeno-associated virus vectors rescues thalamic neurons after visual cortex lesion in the adult rat. Eur J Neurosci. 15:1271–1277.

Cruz-Martín A, El-Danaf RN, Osakada F, Sriram B, Dhande OS, Nguyen PL, Callaway EM, Ghosh A, Huberman AD. 2014. A dedicated circuit links direction-selective retinal ganglion cells to the primary visual cortex. Nature. 507:358–361.

Deck M, Lokmane L, Chauvet S, Mailhes C, Keita M, Niquille M, Yoshida M, Yoshida Y, Lebrand C, Mann F, et al. 2013. Pathfinding of corticothalamic axons relies on a rendezvous with thalamic projections. Neuron. 77:472–484.

Denman DJ, Contreras D. 2015. Complex effects on in vivo visual responses by specific projections from mouse cortical layer 6 to dorsal lateral geniculate nucleus. J Neurosci. 35:9265–9280.

Feldheim DA, O'Leary DDM. 2010. Visual map development: bidirectional signaling, bifunctional guidance molecules, and competition. Cold Spring Harb Perspect Biol. 2:a001768.

Feller MB. 2009. Retinal waves are likely to instruct the formation of eye-specific retinogeniculate projections. Neural Develop. 4:24.

French CA, Fisher SE. 2014. What can mice tell us about Foxp2 function? Curr Opin Neurobiol. 28:72–79.

Fries W. 1985. Inputs from motor and premotor cortex to the superior colliculus of the macaque monkey. Behav Brain Res. 18:95–105.

Fujiyama F, Hioki H, Tomioka R, Taki K, Tamamaki N, Nomura S, Okamoto K, Kaneko T. 2003. Changes of immunocytochemical localization of vesicular glutamate transporters in the rat

visual system after the retinofugal denervation. J Comp Neurol. 465:234–249.

Fukuda T, Kawano H, Ohyama K, Li HP, Takeda Y, Oohira A, Kawamura K. 1997. Immunohistochemical localization of neurocan and L1 in the formation of thalamocortical pathway of developing rats. J Comp Neurol. 382:141–152.

Grant E, Hoerder-Suabedissen A, Molnár Z. 2016. The regulation of corticofugal fiber targeting by retinal inputs. Cereb Cortex. 26:1336–1348.

Han W, Kwan KY, Shim S, Lam MMS, Shin Y, Xu X, Zhu Y, Li M, Sestan N. 2011. TBR1 directly represses Fezf2 to control the laminar origin and development of the corticospinal tract. Proc Natl Acad Sci USA. 108:3041–3046.

Hevner RF, Miyashita-Lin E, Rubenstein JL. 2002. Cortical and thalamic axon pathfinding defects in Tbr1, Gbx2, and Pax6 mutant mice: evidence that cortical and thalamic axons interact and guide each other. J Comp Neurol. 447:8–17.

Hofmann Y, Wirth B. 2002. hnRNP-G promotes exon 7 inclusion of survival motor neuron (SMN) via direct interaction with Htra2-beta1. Hum Mol Genet. 11:2037–2049.

Huberman AD, Feller MB, Chapman B. 2008. Mechanisms underlying development of visual maps and receptive fields. Annu Rev Neurosci. 31:479–509.

Jacobs EC, Campagnoni C, Kampf K, Reyes SD, Kalra V, Handley V, Xie YY, Hong-Hu Y, Spreur V, Fisher RS, et al. 2007. Visualization of corticofugal projections during early cortical development in a tau-GFP-transgenic mouse. Eur J Neurosci. 25:17–30.

Kalil RE, Behan M. 1987. Synaptic reorganization in the dorsal lateral geniculate nucleus following damage to visual cortex in newborn or adult cats. J Comp Neurol. 257:216–236.

Kawamoto S, Niwa H, Tashiro F, Sano S, Kondoh G, Takeda J, Tabayashi K, Miyazaki J. 2000. A novel reporter mouse strain that expresses enhanced green fluorescent protein upon Cre-mediated recombination. FEBS Lett. 470:263–268.

Kim SH, Won SJ, Mao XO, Jin K, Greenberg DA. 2006. Molecular mechanisms of cannabinoid protection from neuronal excitotoxicity. Mol Pharmacol. 69:691–696.

Li Q, Lee J-A, Black DL. 2007. Neuronal regulation of alternative pre-mRNA splicing. Nat Rev Neurosci. 8:819–831.

López-Bendito G, Chan C-H, Mallamaci A, Parnavelas J, Molnár Z. 2002. Role of Emx2 in the development of the reciprocal connectivity between cortex and thalamus. J Comp Neurol. 451: 153–169.

Mende Y, Jakubik M, Riessland M, Schoenen F, Rossbach K, Kleinridders A, Kohler C, Buch T, Wirth B. 2010. Deficiency of the splicing factor Sfrs10 results in early embryonic lethality in mice and has no impact on full-length SMN/Smn splicing. Hum Mol Genet. 19:2154–2167.

Nakamura K, Hioki H, Fujiyama F, Kaneko T. 2005. Postnatal changes of vesicular glutamate transporter (VGluT)1 and VGluT2 immunoreactivities and their colocalization in the mouse forebrain. J Comp Neurol. 492:263–288.

Osterhout JA, Josten N, Yamada J, Pan F, Wu S.-w., Nguyen PL, Panagiotakos G, Inoue YU, Egusa SF, Volgyi B, et al. 2011. Cadherin-6 mediates axon-target matching in a non-image-forming visual circuit. Neuron. 71:632–639.

Osterhout JA, Stafford BK, Nguyen PL, Yoshihara Y, Huberman AD. 2015. Contactin-4 mediates axon-target specificity and functional development of the accessory optic system. Neuron. 86:985–999.

Pak W, Hindges R, Lim Y-S, Pfaff SL, O'Leary DDM. 2004. Magnitude of binocular vision controlled by islet-2 repression of a genetic program that specifies laterality of retinal axon pathfinding. Cell. 119:567–578.

Pfeiffenberger C, Cutforth T, Woods G, Yamada J, Rentería RC, Copenhagen DR, Flanagan JG, Feldheim DA. 2005. Ephrin-As and neural activity are required for eye-specific patterning during retinogeniculate mapping. Nat Neurosci. 8: 1022–1027.

Roberts JM, Ennajdaoui H, Edmondson C, Wirth B, Sanford JR, Chen B. 2014. Splicing factor TRA2B is required for neural progenitor survival. J Comp Neurol. 522:372–392.

Seabrook TA, El-Danaf RN, Krahe TE, Fox MA, Guido W. 2013. Retinal input regulates the timing of corticogeniculate innervation. J Neurosci. 33:10085–10097.

Shanks JA, Ito S, Schaevitz L, Yamada J, Chen B, Litke A, Feldheim DA. 2016. Corticothalamic axons are essential for retinal ganglion cell axon targeting to the mouse dorsal lateral geniculate nucleus. J Neurosci. 36:5252–5263.

Storbeck M, Hupperich K, Gaspar JA, Meganathan K, Martínez Carrera L, Wirth R, Sachinidis A, Wirth B. 2014. Neuronal-specific deficiency of the splicing factor Tra2b causes apoptosis in neurogenic areas of the developing mouse brain. PLoS One. 9:e89020.

Su J, Haner CV, Imbery TE, Brooks JM, Morhardt DR, Gorse K, Guido W, Fox MA. 2011. Reelin is required for class-specific retinogeniculate targeting. J Neurosci. 31:575–586.

Wang Q, Burkhalter A. 2013. Stream-related preferences of inputs to the superior colliculus from areas of dorsal and ventral streams of mouse visual cortex. J Neurosci. 33: 1696–1705.

Watermann DO, Tang Y, Zur Hausen A, Jäger M, Stamm S, Stickeler E. 2006. Splicing factor Tra2-beta1 is specifically induced in breast cancer and regulates alternative splicing of the CD44 gene. Cancer Res. 66:4774–4780.

Weller R, Kaas J. 1980. Loss of retinal ganglion cells and altered retinogeniculate projections in monkeys with striate cortex lesions. Invest Ophthal Vis Sci. 19:2.

Weller RE, Kaas JH, Ward J. 1981. Preservation of retinal ganglion cells and normal patterns of retinogeniculate projections in prosimian primates with long-term ablations of striate cortex. Invest Ophthalmol Vis Sci. 20:139–148.

Wilkes M, Zingaro G, Murphy EH. 1985. Survival of the ganglion cell population in the rabbit retina following neonatal visual cortex ablation. Brain Res. 353:293–297.

Xu HP, Furman M, Mineur YS, Chen H, King SL, Zenisek D, Zhou ZJ, Butts DA, Tian N, Picciotto MR, et al. 2011. An instructive role for patterned spontaneous retinal activity in mouse visual map development. Neuron. 70:1115–1127.

Zhang J, Ackman JB, Xu HP, Crair MC. 2012. Visual map development depends on the temporal pattern of binocular activity in mice. Nat Neurosci. 15:298–307.